

# CrystEngComm

Accepted Manuscript



This is an *Accepted Manuscript*, which has been through the Royal Society of Chemistry peer review process and has been accepted for publication.

*Accepted Manuscripts* are published online shortly after acceptance, before technical editing, formatting and proof reading. Using this free service, authors can make their results available to the community, in citable form, before we publish the edited article. We will replace this *Accepted Manuscript* with the edited and formatted *Advance Article* as soon as it is available.

You can find more information about *Accepted Manuscripts* in the [Information for Authors](#).

Please note that technical editing may introduce minor changes to the text and/or graphics, which may alter content. The journal's standard [Terms & Conditions](#) and the [Ethical guidelines](#) still apply. In no event shall the Royal Society of Chemistry be held responsible for any errors or omissions in this *Accepted Manuscript* or any consequences arising from the use of any information it contains.

Cite this: DOI: 10.1039/c0xx00000x

www.rsc.org/xxxxxx

ARTICLE TYPE

# Morphological control of RGO/CdS hydrogel for energy storage

Xueyu Zhang, Xin Ge\*, Shihan Sun, Yuanduo Qu, Wenzhong Chi, Chuandong Chen and Wei Lü\*

Received (in XXX, XXX) Xth XXXXXXXXX 20XX, Accepted Xth XXXXXXXXX 20XX

DOI: 10.1039/b000000x

5 As a newly developed material system, graphene based three-dimensional (3D) architectures have been receiving considerable attention due to their multifunctional properties. Herein, we explore the synergic effect of combined CdS and graphene hybrids in 3D architecture, and investigate its application in electrochemical energy storage. A facile hydrothermal procedure is used to prepare 3D reduced graphene oxide/CdS (RGO/CdS) hydrogels, and three different morphologies of CdS (ball-like, rod-like, needle-  
10 like) in the hydrogels are obtained by controlling synthesis conditions. The results showed that the morphology of CdS significantly affects the electrochemical properties of RGO/CdS. The electrode prepared with needle-like CdS nanoparticles exhibited the highest specific capacitor value of 300 F/g at a scan rates 5 mV/s, which shows outstanding cycling stability with 94% of the capacitance retention after 1000 cycles of charge/discharge. These findings demonstrate the possibility of 3D RGO/CdS architecture  
15 for application in energy storage.

## 1. Introduction

With the increasing energy demand in applications for portable electronics, hybrid vehicles and industrial equipment, great efforts have been devoted in designing and developing the novel  
20 materials for energy storage. Supercapacitors have received great attention due to their excellent properties such as high power, long cyclic life, and fast charge/discharge rates.<sup>1-3</sup> Generally, three types of materials have been extensively investigated as electrode materials in supercapacitor devices: carbon materials,  
25 metal oxides and conducting polymers. Carbon based materials, including carbon nanotubes,<sup>4-7</sup> activated carbon,<sup>8-10</sup> and graphene nanosheets,<sup>11-13</sup> have been used as electrode materials in supercapacitors. Among them, graphene has attracted great scientific and technological interests due to high theoretical  
30 surface area, excellent electronic conductivity, and strong mechanical strength. Recently, porous 3D graphene based hybrid structures, have been intensively investigated because of their unique inherent properties; their porous structures have higher surface area and inner space for the transportation or storage of  
35 electrons/ions and electrolyte compared with original graphene sheets.<sup>14</sup> Graphene-based 3D architectures such as RuO<sub>2</sub>,<sup>15</sup> MnO<sub>2</sub>,<sup>16</sup> V<sub>2</sub>O<sub>5</sub>,<sup>16,17</sup> Fe<sub>3</sub>O<sub>4</sub>,<sup>18</sup> and NiS<sup>19</sup> etc have been prepared to investigate the potential applications for energy storage.

CdS as a typical II-VI semiconductors exhibit the size-  
40 dependent nonlinear optical, physical and electronic properties, which make it promising materials and provide possibilities of applications in several fields. Since Cao et al. reported the synthesis of reduced graphene oxide/CdS (RGO/CdS) nanocomposites,<sup>20</sup> numerous researches for applications of  
45 RGO/CdS in photocatalyst and electrochemical biosensor<sup>21-23</sup> have been reported. However, few research has been reported on

RGO/CdS nanocomposite for its electrocatalytic behavior and supercapacitor electrodes. In addition, we expect the combination of porous 3D structures, the excellent intrinsic properties of  
50 graphene and synergistic effect of CdS in the composites would induce improved electrochemical behaviors.

In present work, we investigated the preparation of 3D RGO/CdS hydrogels by a facile hydrothermal process, morphology control of CdS (ball-like, rod-like, needle-like) in 3D  
55 structures, and application in electrochemical energy storage. The results exhibit that the morphology of CdS significantly affects the electrochemical properties of RGO/CdS. The electrode prepared with needle-like CdS nanoparticles exhibited the highest specific capacitor value of 300 F/g at a scan rates 5 mV/s, which  
60 shows outstanding cycling stability with 94% of the capacitance retention after 1000 cycles of charge/discharge. These findings demonstrate the possibility of 3D RGO/CdS architecture for application in energy storage.

## 2. Materials and methods

### 2.1 Chemicals

All the chemicals and reagents were of analytical purity and used without further purifications. L-Cys, cadmium nitrate (Cd(NO<sub>3</sub>)<sub>2</sub>·4H<sub>2</sub>O) and Ethylenediamine (EDA) were purchased from Aladdin. Water used in all experiments was doubly distilled  
70 and purified by a Milli-Qsystem (Billerica, MA, USA).

### 2.2 Synthesis of CdS

Typically, 30 mL of a mixed solvent containing water and EDA with a certain ratio (the ratio of EDA to water: 0/30, 5/30, 15/30) were added into the mixture of 0.5 mmol Cd(NO<sub>3</sub>)<sub>2</sub>·4H<sub>2</sub>O and 0.5  
75 mmol L-Cys to get a muddy solution, followed by 30 min stirring. The solution was then transferred into a Teflon-lined

stainless steel autoclave (50mL) and reacted under 160 °C for 12 h. After cooling to room temperature, the obtained solution was centrifuged and washed by deionized water several times. Finally, the formed CdS composites were dried in a vacuum drier.

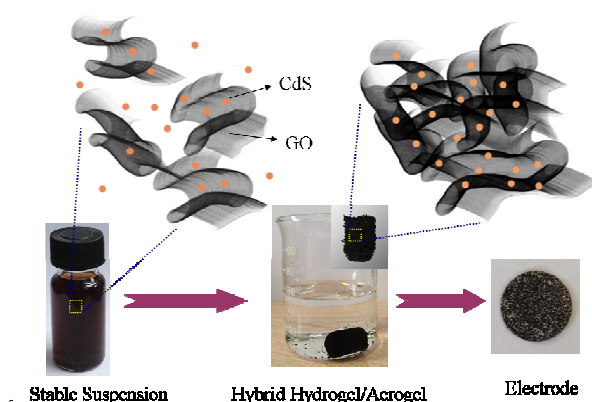


Figure 1 Schematic illustration of the synthetic procedures for RGO/CdS

### 2.3 Synthesis of RGO/CdS nanocomposites

Graphite oxide (GO) was synthesized from natural graphite powder according to the modified Hummers method.<sup>24</sup> Subsequently, 50 mg of as-prepared CdS nanoparticles (NPs) was dispersed in 30 ml GO aqueous solution (2 mg/ml), which was left to stir for 30 min. The solution was subjected to hydrothermal process (180 °C for 12 h), followed by a quickly frozen procedure with liquid nitrogen. Then the RGO/CdS NPs composite (aerogel) was formed by freeze-drying process in a freeze drier. The detailed preparation procedure is shown in Figure 1.

### 2.4 Instrumental and analytical conditions

The microstructures of the composite samples were investigated by transmission electron microscopy (TEM) with JEOL2010. The powder X-ray diffraction (XRD) measurements were performed using a D-MAX II A X-ray diffractometer with CuK $\alpha$  radiation ( $\lambda = 1.5406 \text{ \AA}$ ). The X-ray photoelectron spectroscopy (XPS) measurements were conducted with a VG ESCALAB MKII spectrometer. Fourier transform infrared spectroscopy (FTIR) spectra were recorded on a VERTEX 70 spectrometer.

### 2.5 Electrochemical measurements

The test electrodes were prepared by mixing active materials with conductive carbon black as the conductive agent and polyvinylidene fluoride (PVDF) dissolved in N-methyl-2-pyrrolidone (NMP) as the binder in a weight ratio of 8:1:1 to

form a slurry, which was then coated onto Nickel foam. All electrochemical characteristics were evaluated by cyclic voltammetry (CV), galvanostatic charge/discharge and electrochemical impedance spectroscopy (EIS) measurements on an IVIUMSTAT electrochemical workstation. The CVs were performed in a voltage window between -1.0 and 0 V at different scan rates. The galvanostatic charge/discharge were carried out in a voltage window between -1.0 and 0 V under different current density from 0.5 A/g to 10 A/g. The EISs were investigated in the frequency range from 100 KHz to 0.01 Hz at open circuit voltage by applying a 14.14 mV signal. All measurements were taken using 6 M KOH as electrolyte at room temperature.

## 3 Results and discussion

Figure 2 shows the SEM images of the three samples with different EDA addition amount. For all three samples, the graphene sheets are formed with several micrometers in size, and CdS particles are assembled and well distributed on the graphene

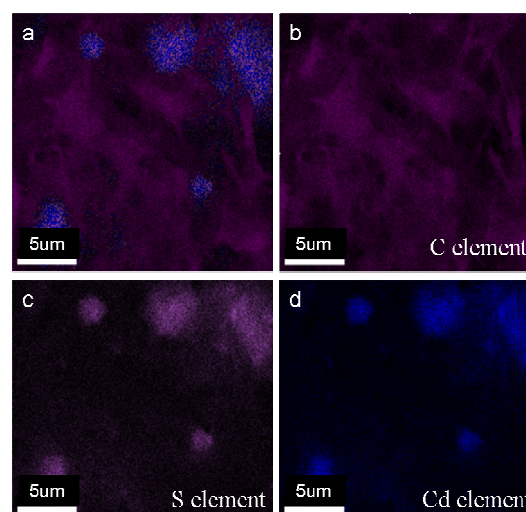


Figure 3 (a) Elements mapping of RGO/CdS areogel (EDA:5/30), (b) C element, (c) S element, (d) Cd element.

sheets, which has wrinkles and folded regions on the edge. The three samples exhibit interconnected, porous 3D graphene framework with continuous macropores in the micrometer size range. Figure 3 shows the element distribution taken from

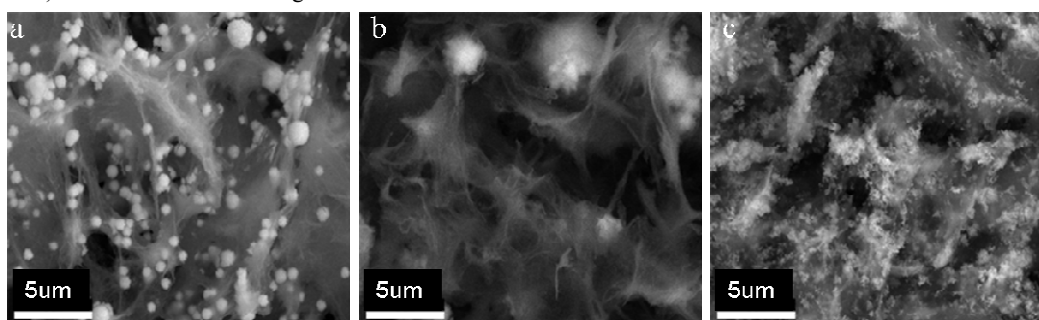


Figure 2 SEM image of RGO/CdS prepared with different EDA ratio 0/30 (a), 5/30 (b), 15/30 (c).

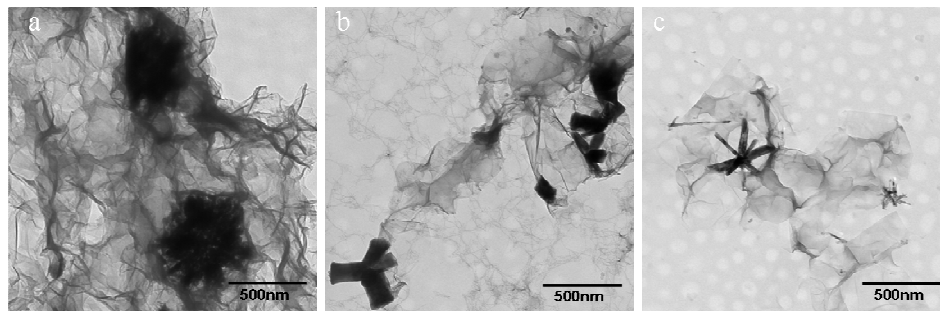


Fig.4 TEM image of RGO/CdS NPs prepared with different EDA ratio 0/30 (a), 5/30 (b), 15/30 (c).

Figure 2b, which confirms the existence of C, S, and Cd in the structure. The S and Cd occupy the same position corresponding to the position of white particles in Figure 2b, indicating the formation of CdS NPs. From SEM images, it could be observed that the morphologies of the three samples are different. The three samples have nest-like structures of the CdS which packed or adhered on both sides of graphene sheets. The detail structure is further proved by TEM observation as shown in Figure 3. Without EDA addition, the nest-like structure of the CdS component is formed by many nanospheres with 400 nm average size as shown in Figure 3a. With the increasing EDA amount, the nest-like structure of the CdS component changes from nanorods with 50 nm in diameter (Figure 3b) to nanowires with 10 nm in diameter (Figure 3c). Therefore, we defined the three samples to be ball-like, rod-like, and needle-like, respectively.

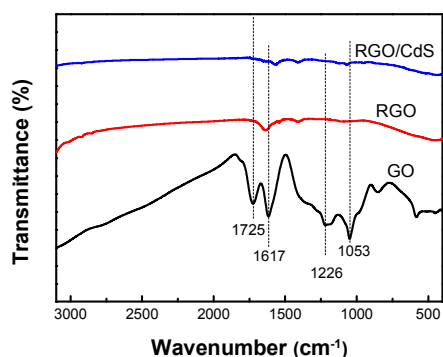


Figure 5 FTIR spectra of GO, CdS and RGO/CdS.

FTIR has been used to identify the surface functional groups of the samples. Since the results of the three samples are very similar, only needle-like RGO/CdS curve is present here. As shown in Figure 5, while GO keeps many feature peaks related to oxygen including functional group, the peaks of RGO and RGO/CdS at 1053  $\text{cm}^{-1}$ , 1226  $\text{cm}^{-1}$  and 1725  $\text{cm}^{-1}$ , corresponding to C-O stretching vibrations, the phenolic C-OH stretching and C=O stretching peak<sup>25-27</sup> disappear, which indicates that the GO is reduced into graphene in hydrothermal process.

XRD are used to investigate the crystallinity. As shown in Figure 6, the diffraction peaks of the RGO/CdS composites are well indexed to crystal planes of a hexagonal phase CdS, which demonstrates that the CdS component in RGO/CdS composites is formed into a pure hexagonal phase with high crystallinity. In addition, no diffraction peak of GO could be found in RGO/CdS composites, suggesting that the GO has been reduced into

graphene nanosheets, which is consistent with FTIR results.

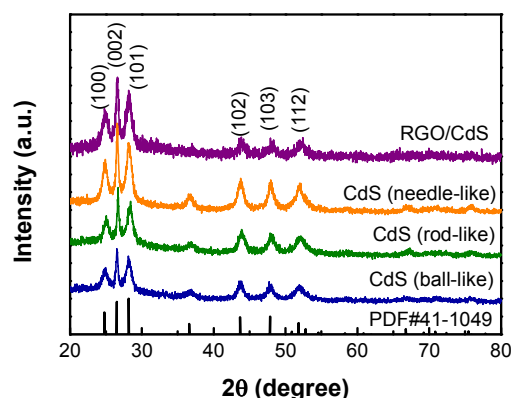


Figure 6 XRD picture of GO, CdS and RGO/CdS.

Figure 7a shows the XPS surveys of GO and needle-like RGO/CdS. The C and O elements in the three samples were observed by the photoelectron lines at binding energies of about 285 and 711 eV which are attributed to C 1s and O 1s, respectively. O1s peaks of needle-like RGO/CdS are obviously decreased as compared to that of GO in the wide region, and the oxygen signal in the survey spectrum can be related to air contamination due to ex situ analysis, suggesting that the C/O ratio increases remarkably after hydrothermal process. This could be confirmed by the deconvoluted C 1s spectra as shown in Figure 7b. The deconvoluted C 1s spectra show the presence of four different carbon groups: graphitic carbon at 284.6 eV (C=C), alcohol, phenolic, and ether groups at 286.5 eV (C-O), the carbonyl carbon at 287.9 eV (C=O), and ester or carboxyl groups at 288.4 eV (C=O-C)<sup>28</sup>. Compared with the C 1s spectrum of GO, the oxygen related peaks in the needle-like RGO/CdS are much weaker suggesting most of GO had been reduced in the hydrothermal process.

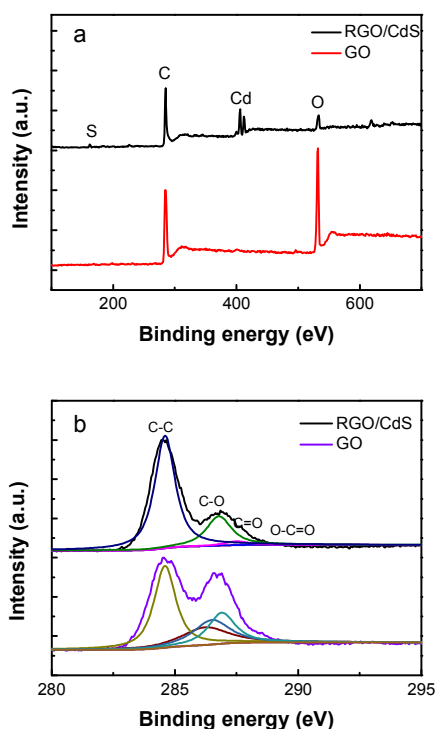


Figure 7 (a) XPS surveys of GO and needle-like RGO/CdS, (b) XPS C 1s spectrum of GO and needle-like RGO/CdS.

To evaluate the electrochemical performance of RGO/CdS active materials, a typical three-electrode mode measurement is constructed in this work. Figure 8a shows the CV curves of RGO electrodes. With the increasing scan rates from 5 to 200 mV/s, the CV curves retain the rectangular shape showing the ideal electrochemical double layer behavior. The specific capacitances of active materials obtained from the CV curves can be calculated by the equation<sup>25</sup>:

$$C = \left( \int I dv \right) / (vmV) \quad (1)$$

where  $I$  is the current (A),  $V$  is the potential window (V),  $v$  is the scan rate (mV/s) and  $m$  is the mass of the active materials (g).

Figure 8b shows the specific capacitance values of RGO and RGO/CdS with different morphologies. The specific capacitance of ball-like sample is even lower than that of RGO, which is probably due to the pure crystalline quality of ball-like CdS and the large mass percentage of CdS in hybrids. Compared with RGO, the specific surface area of RGO/CdS is small, which bring down the specific capacitance of electrode. However, both the specific capacitance values of with rod-like and needle-like RGO/CdS samples are higher than that of the RGO. The obvious increase of electrochemical capacitance of RGO/CdS compared with the RGO was ascribed to the faradic contribution of CdS nanoparticles to EDLC of RGO. The morphology of CdS nanoparticle has remarkable influence on the specific capacitance of RGO/CdS electrodes. The maximum value of 300 F/g (5mV/s) is achieved by needle-like RGO/CdS. Since the needle-like RGO/CdS electrode got the maximum specific capacitance, the electrochemical properties of the as-prepared RGO/CdS (needle-like) electrodes had been further studied by CV, galvanostatic charge/discharge, Cycling stability and EIS. The CV and

galvanostatic charge/discharge curves of the needle-like RGO/CdS electrode are shown in Figure 9a and 9b, respectively.

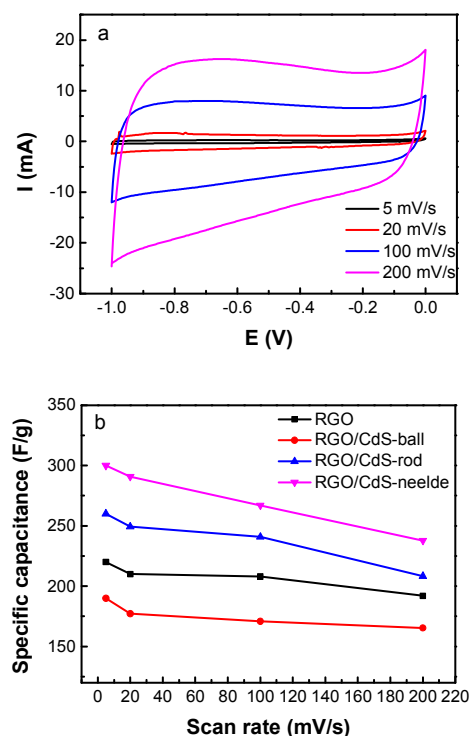


Figure 8 (a) DC curves of RGO electrode, (b) Specific capacitance of 40 different electrodes as function of scan rate.

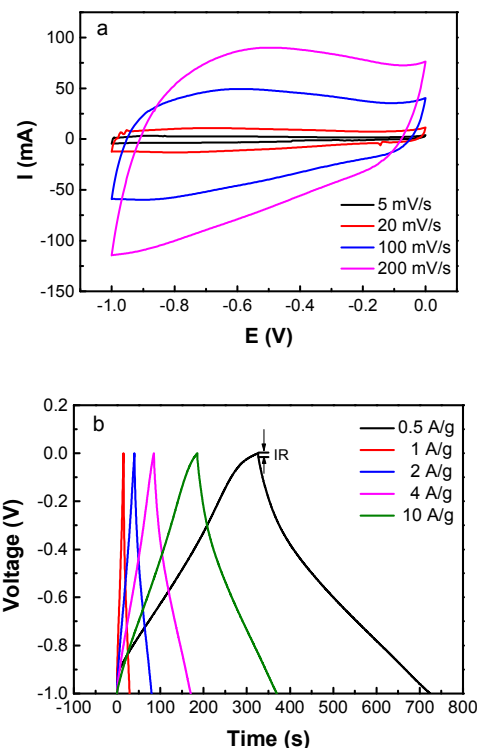


Figure 9 CV (a) and Galvanostatic charge/discharge (b) curves of the RGO/CdS (needle-like) electrode.

The galvanostatic charge/discharge curves exhibit almost triangular shape with a small internal resistance (IR) drop at current density of 0.5 A/g, implying a high degree of symmetry in charge and discharge.<sup>29</sup> The presence of the IR drop at the beginning of discharge is relevant to the equivalent series resistance of the electrode.<sup>30</sup> According to the galvanostatic charge/discharge results, the specific capacitance of RGO/CdS nanocomposite can be calculated by the equation<sup>31</sup>:

$$C = (I\Delta t) / (m\Delta V) \quad (2)$$

where  $I$  is the constant discharge current (A),  $\Delta t$  is the discharge time (s), and  $\Delta V$  is the discharge voltage excluding the IR drop (V). The specific capacitance of RGO/CdS nanocomposite from discharge curve (0.5 A/g) is calculated to be 204 F/g.

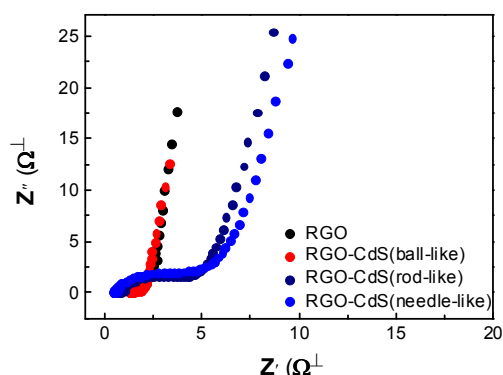


Figure 10 EIS of RGO and RGO/CdS electrodes.

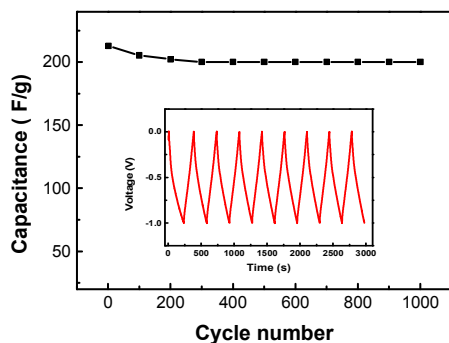


Figure 11 Cycle performance of RGO/CdS (needle-like) electrode at current density of 1 A/g. Inset shows the first 10 cycles of galvanostatic charge-discharge.

The different charge storage mechanisms of RGO and RGO/CdS (different morphology) electrodes are also evident from the EIS analysis as shown in Figure 10. It can be observed that the Nyquist plots have two distinct parts, a semicircle part at high frequency and a linear part at low frequency. The RGO and RGO/CdS (ball-like) electrodes exhibit two almost vertical line along the imaginary axis in the low-frequency region, indicating they are ideally capacitive behavior without Faradic charge storage mechanism. However, the RGO/CdS (rod-like and needle-like) electrodes show more inclined curve in the low frequency region, suggesting the predominance of pseudocapacitance. Cycling stability is an important factor in supercapacitor operation. The repetitive charge/discharge test of

the needle-like RGO/CdS electrode at current density of 1 A/g over 1000 cycles was carried out. The cyclic test shows that the active material maintains ~94% of the initial capacitance after 1000 cycles indicating its good stability as shown in Figure 11.

Currently, addition of conducting polymers or transition metal compounds are two efficient strategies for improving the specific capacitance of graphene-based supercapacitors. Compared with graphene/conducting polymers composite, the RGO/CdS structure exhibits improved cyclic stability, which is similar with that of RGO/MnO<sub>2</sub> and RGO/Fe<sub>3</sub>O<sub>4</sub>.<sup>32-34</sup> As a morphology controllable materials, we have reason to believe that the electrochemical properties of RGO/CdS can be improved with the modified of electrode structure and preparation method.

## 4. Conclusions

In summary, we have synthesized 3D RGO/CdS hydrogel for application in electrochemical energy storage. The morphologies of CdS in hybrid structures could be chemically adjusted. The results showed that the morphologies of CdS significantly affect the electrochemical properties of RGO/CdS. The electrode prepared with needle-like RGO/CdS exhibited the highest specific capacitor value of 300 F/g at a scan rates 5 mV/s, which shows outstanding cycling stability with 94% of the capacitance retention after 1000 cycles of charge/discharge. Present work enlarges the application of CdS nanomaterial, some new devices may be invented based on this work.

## Acknowledgements

Financial support from the National Natural Science Foundation of China (authorization numbers: 61376020, 21301167, 61574021), Science and Technology Department of Jilin Province (20130101009JC, 20140414024GH), Education Department of Jilin Province(2015-94), Innovation Scientists and Technicians Troop Construction Projects of Changchun City (201417214GH016), China are acknowledged.

## Notes and references

- 1 J. R. Miller, P. Simon, *Science*, 2008, **321**, 651.
- 2 P. Simon, Y. Gogotsi, *Nat. Mater.* 2008, **7**, 845.
- 3 C. Liu, F. Li, L. P. Ma, H. M. Cheng, *Adv. Mater.* 2010, **22**, E28.
- 4 H. Pan, J. Li and Y. P. Feng, *Nanoscale Res. Lett.*, 2010, **5**, 654.
- 5 R. A. Fisher, M. R. Watt and W. J. Ready, *ECS J. Solid State Sci. Technol.*, 2013, **2**, M3170.
- 6 V. V. Obreja, *Phys. E.*, 2008, **40**, 2596.
- 7 E. Frackowiak and F. Beguin, *Carbon*, 2001, **39**, 937.
- 8 F. Markoulidis, C. Lei, C. Lekakou, E. Figgemeier, D. Duff, S. Khalil, B. Martorana and I. Cannavaro, *IOP Conf. Ser.: Mater. Sci. Eng.*, 2012, **40**, 012021.
- 9 D. Saha, Y. Li, Z. Bi, J. Chen, J. K. Keum, D. K. Hensley, H. A. Grappe, H. M. Meyer, S. Dai, M. P. Paranthaman and A. K. Naskar, *Langmuir*, 2014, **30**, 900.
- 10 C. Liang, Z. Li and S. Dai, *Angew. Chem., Int. Ed.*, 2008, **47**, 3696.

- 11 D. Sun, X. Yan, J. Lang and Q. Xue, *J. Power Sources*, 2013, **222**, 52.
- 12 M. D. Stoller, S. Park, Y. Zhu, J. An and R. S. Ruoff, *Nano Lett.*, 2008, **8**, 3498.
- 13 X.Y. Peng, X.X. Liu, D. Diamond and K. T. Lau, *Carbon*, 2011, **49**, 3488.
- 14 W. Wang, S. Guo, M. Penchev, I. Ruiz, K. N. Bozhilov, D. Yan, M. Ozkan and C. S. Ozkan, *Nano Energy*, 2013, **2**, 294.
- 15 W. Dmowski, T. Egami, K. E. Swider-Lyons, C. T. Love and D. R. Rolison, *J. Phys. Chem. B*, 2002, **106**, 12677.
- 16 B. Saravanakumar, K. K. Purushothaman and G. Muralidharan, *CrystEngComm*, 2014, **16**, 10711.
- 17 T. Peng, J. Wang, Q. Liu, J. Liu and P. Wang, *CrystEngComm*, 2015, **17**, 1673.
- 18 K. Chen, X. Chen and D. Xue, *CrystEngComm*, 2015, **17**, 1906.
- 19 H. M. Zhang, X. Z. Yu, D. Guo, B. H. Qu, M. Zhang, Q. H. Li and T. H. Wang, *ACS Appl. Mater. Interfaces*, 2013, **5**, 7335.
- 20 A. Cao, Z. Liu, S. Chu, M. Wu, Z. Ye, Z. Cai, Y. Chang, S. Wang, Q. Gong, and Y. Liu *Adv. Mater.* 2010, **22**, 103.
- 21 T. T. Yang, W. T. Chen, Y. J. Hsu, K. H. Wei, T.Y. Lin, T. W. Lin, *J. Phys Chem C*, 2010, **114**, 11414.
- 22 S. Y. Ryu, W. Balcerski, T. K. Lee, M. R. Hoffmann, *J Phys Chem C*, 2007, **111**, 18195.
- 23 H. Zhang, Y. F. Zhu, *J Phys Chem C*, 2010, **114**, 5822.
- 24 M. D. Stoller, S. J. Park, Y. W. Zhu, J. H. An and R. S. Ruoff, *Nano Lett.*, 2008, **8**, 3498.
- 25 X. L. Wu, T. Wen, H. L. Guo, S. Yang, X. Wang, and A. Xu, *ACS NANO*, 2013, **7**, 3589.
- 26 X. Sun, Y. Li, *Angew. Chem., Int. Ed.* 2004, **43**, 597.
- 27 B. Grzyb, C. Hildenbrand, S. Berthon-Fabry, D. Bégin, N. Job, A. Rigacci, P. Achard, *Carbon* 2010, **48**, 2297.
- 28 H. P. Cong, X. C. Ren, P. Wang, S. H. Yu, *ACS Nano* 2012, **6**, 2693.
- 29 H. Wang, Z. Liu, X. Chen, P. Han, S. Dong, G. Cui, *J. Solid State Electrochem.* 2011, **15**, 1179.
- 30 Z. Lei, F. Shi, L. Lu, *ACS Appl. Mater. Interfaces* 2012, **4**, 1058.
- 31 B. G. Choi, M. H. Yang, W. H. Hong, J. W. Choi, Y. S. Huh, *ACS Nano* 2012, **6**, 4020.
- 32 G. Zhu, Z. He, J. Chen, J. Zhao, X. Feng, Y. Ma, Q. Fan, L. Wang, W. Huang, *Nanoscale*, 2014, **6**, 1079.
- 33 J. P. Cheng, Q. L. Shou, J. S. Wu, F. Liu, V. P. Dravid, X. B. Zhang, *J. Electroanal. Chem.*, 2013, **698**, 1.
- 34 Q. H. Wang, L. F. Jiao, H. M. Du, Y. J. Wang and H. T. Yuan, *J. Power Sources*, 2014, **245**, 101.

## Graphical Abstract

The paper investigated the preparation of 3D RGO/CdS hydrogels by a facile hydrothermal process, morphology control of CdS (ball-like, rod-like, needle-like) in 3D structures, and application in electrochemical energy storage.

